Journal of Alloys and Compounds 515 (2012) 57–62

Contents lists available at SciVerse ScienceDirect

Journal of Alloys and Compounds

journal homepage: www.elsevier.com/locate/jallcom

Electrodeposition of arborous structure nanocrystalline SnO_2 and application in flexible dye-sensitized solar cells

Zeng Chen [a], Yafang Tian [b], Shengjun Li [a], Haiwu Zheng [a], Weifeng Zhang [a,*]

[a] Key Laboratory of Photovoltaic Materials of Henan Province and School of Physics & Electronic, Henan University, Kaifeng 475001, People's Republic of China
[b] Training Center of Zhengzhou Railway Vocational & Technical College, Zhengzhou 450052, People's Republic of China

ARTICLE INFO

Article history:
Received 25 July 2011
Received in revised form 24 October 2011
Accepted 29 October 2011
Available online 18 November 2011

Keywords:
Flexible dye-sensitized solar cells
Electrodeposition
SnO_2
Pulse-potential technique

ABSTRACT

Arborous structure SnO_2 porous films were electrodeposited on Ti substrate using pulse-potential technique. The deposition process of SnO_2 was investigated through cyclic voltammetry, potentiostatic electrolysis and chronoamperometry. It was found that SnO_2 and metallic Sn were codeposited under the low pulse potential (−0.6 V *vs.* Ag/AgCl). The electrodeposited Sn was anodic oxidized under the subsequent high pulse potential (−0.1 V *vs.* Ag/AgCl). The formation of SnO_2 possessed an instantaneous nucleation process. Dye-sensitized solar cells were fabricated using the electrodeposited SnO_2 porous films. The photo-electricity conversion efficiency was about 0.47%.

1. Introduction

Dye-sensitized solar cells (DSCs) have attracted great scientific and technological interests as photovoltaic devices for their utilization of non-toxic materials, simple preparation process and high photoelectric conversion efficiency up to 11% [1–4]. The highest energy conversion efficiencies have been achieved by the photoelectrode based on nanocrystal TiO_2. However, the organic solvent in DSCs might decompose with the catalyzing of TiO_2 under UV light which will bring down the long term stability [5,6]. Other semiconductors, such as SnO_2, ZnO, Nb_2O_5 and WO_3, have also been employed as photoanode materials for DSCs [7–11]. SnO_2 has been extensively used in transparent conduction glass, gas sensors, lithium ion batteries for its transparent property and high electronic mobility [12–15]. As an n-type semiconductor with wide band gap (about 3.8 eV), the application of SnO_2 in DSCs might reduce the effect of UV light in natural light on the performance of solar cell and improves the long term stability [16].

To achieve high quality nanoporous photoelectrode, various methods have been developed, such as hydrothermal synthesis, chemical vapor deposition, physical vapor deposition, electrodeposition, etc. [17–19]. In contrast with other techniques, the electrodeposition method was usually carried out under 100 °C and could give rigid control on film thickness and composition. Various metal oxides, such as TiO_2, ZnO, In_2O_3, and ZrO_2, had been successfully electrodeposited [19–22]. At the same time, the electrodeposited TiO_2 and ZnO films had been extensively studied in dye-sensitized solar cells. Lin et al. [23] electrodeposited ZnO nanobelt which showed a short circuit current as high as 17 mA cm^{-2}. An et al. [24] introduced CTAB into the electrolyte as surfactant and obtained thick and crack-free TiO_2 electrode for DSCs. During the electrodeposition process, the electrons keep flowing through the nanoporous film. So the electrodeposited electrode is expected to possess fine electron transport properties even without high temperature sintering. Wessels [20] and Karuppuchamy [25] investigated the photoelectric properties of the TiO_2 and ZnO, respectively, which were used as photoanode without calcination.

Chang et al. [26–28] had electrodeposited SnO_2 film on copper disk. This film possessed a large surface area of 34.3 m^2 g^{-1} which showed the potential application in DSCs. In this paper, we studied the deposition process of SnO_2 through cyclic voltammetry, potentiostatic electrolysis and chronoamperometry. Arborous structure SnO_2 porous films were prepared on the titanium sheet by pulse-potential technique. The photoelectric properties of N3 sensitized SnO_2 electrodes were investigated.

2. Experimental

2.1. Preparation and characterization of SnO_2 film

The preparation of nanocrystalline SnO_2 films was carried out with a simple three electrodes system. Ti (thickness of 0.1 mm) and Pt sheet (efficient area 4 cm^2) were used as working and counter electrode, respectively. The distance between the working electrode and the counter electrode was controlled to be about 3.5 cm.

* Corresponding author.
E-mail address: wfzhang@henu.edu.cn (W. Zhang).

0925-8388/$ – see front matter © 2011 Published by Elsevier B.V.
doi:10.1016/j.jallcom.2011.10.116

Ag/AgCl electrode with saturation potassium chloride aqueous solution worked as the reference electrode. The electrolyte consisted of 0.05 M $SnCl_2$ and 0.1 M HNO_3. The deposition temperature was fixed at 75 °C by an oil bath. The Ti sheet which was used as flexible metal substrate for nanocrystalline SnO_2 film was ultrasonically cleaned in detergent solution, acetone and deionized water, sequentially. The exposed surface area of the working electrode was about 1.5 cm^2. Electrochemical deposition experiments were carried out with CHI660 C electrochemical workstation (Shanghai Chen-hua Instrument Co., China). Pulse-potential technique was adopted in the deposition process with a high potential of −0.1 V (*vs.* Ag/AgCl) and a low potential of −0.6 V (*vs.* Ag/AgCl). The pulse time was 10 s and deposition time was 1 h. The deposited samples were cleaned with deionized water and dried in air at room temperature. The dried films were annealed at 450 °C, 550 °C and 650 °C, respectively, for 1 h in the air.

The crystalline phase of the samples was characterized by DX-2500 X-ray diffractometer (XRD) with a monochromatized Cu Kα irradiation (λ = 0.154145 nm). The morphology of samples was determined using a Nova NanoSEM 650 field emission scanning electron microscope (FE-SEM).

2.2. Fabrication and characterization of dye-sensitized solar cells

For DSCs fabrication, the samples were immersed in a 5×10^{-4} mol L^{-1} ethanol solution of *cis*-bis(thiocyanato)-*N*,*N*′-bis(2,2′-bipyridyl-4,4′-dicarboxylate) ruthenium (II) (N3 dye) for 24 h. A transparent Pt counter electrode was prepared by spreading 5 mmol L^{-1} H_2PtCl_6 aqueous solution on an ITO glass substrate and pyrolyzed at 390 °C for 15 min. The mixture of 0.6 M dimethylpropylimidazolium iodide, 0.1 M iodine, 0.5 M 4-*tert*-butylpyridine, and 0.1 M lithium iodide in methoxy acetonitrile was selected to be the electrolyte of DSCs.

The photoelectrochemical characteristics of DSCs were characterized by the photocurrent-voltage curves (*I*–*V* curves) with CHI660C Electrochemical Workstation under the simulated solar light. A 500 W xenon lamp was used as the light source. The incident light intensity was 100 mW cm^{-2} measured by a Radiation Meter (FZ-A, Beijing Normal University, China) and the active cell area was 0.25 cm^2. The absorption and reflectance spectrum were recorded with a UV–vis–IR photospectrometer (Varian Cary 5000).

3. Results and discussion

3.1. Cyclic voltammetry and potentiostatic electrolysis analysis

To clarify the formation mechanism of SnO_2, cyclic voltammetry experiments were performed in (a) 50 mM $SnCl_2$ + 0.1 M HCl (curve a) and (b) 50 mM $SnCl_2$ + 0.1 M HNO_3 (curve b). In this experiment, Pt foil (0.2 cm^2) was used as the working electrode. Similar cyclic voltammograms (CVs) were obtained with one couple of redox peaks shown in Fig. 1. On the cathodic sweep, significant current was observed from the voltage approximately −0.42 V, which corresponded to the deposition of Sn metal. The Sn^{2+} ions could easily be transformed to Sn^{4+} ions by the dissolved oxygen in the solution. Hence, the cathodic current peak on curve (a) is related to the reduction of Sn^{4+}.

After the reversal of sweep direction, an anodic current peak corresponds to the dissolution of Sn metal. There was no significant difference of the deposition potential between HCl and HNO_3 solution. These tests suggest that the formation of Sn is inescapable during the pulse electrodeposition process. Based on the results of cyclic voltammograms, it seems that the deposition proceeds with the same reaction in HCl and HNO_3 solutions. However, the cathodic current peak of curve (b) is much higher than that of curve (a) which should be caused by the reduction of NO_3^-. During the electrodeposition process, no gas bubble was found on the cathodic electrode. So the reduction of NO_3^- might proceed with the following reactions:

$$NO_3^- + H_2O + 2e^- \rightarrow NO_2^- + 2OH^- \quad (1)$$

or

$$NO_3^- + 7H_2O + 8e^- \rightarrow NH_4^+ + 10OH^- \quad (2)$$

The hydroxyl group emerged at the surface of cathodic electrode and reacted with metal ions (Sn^{4+}) coming from the solution to form metal oxide according to Reaction (3):

$$Sn^{4+} + 4OH^- \rightarrow SnO_2 + 2H_2O \quad (3)$$

Fig. 2(a) and (b) shows the voltammograms for Pt electrode at various scan rates in 50 mM $SnCl_2$ + 0.1 M HCl and 50 mM $SnCl_2$ + 0.1 M HNO_3, respectively. It can be seen that the peak current is linearly varying with the square root of scan rate in HCl solution (shown in Fig. 3a). This phenomenon indicates that the reduction of stannic ions on Pt electrode is diffusion controlled process [29]. However, in the HNO_3 solution, the peak current is not directly proportional to the square root of scan root. Accordingly, the electrochemical reduction of stannic cannot be simply described as a diffusion-control reaction for the solution containing

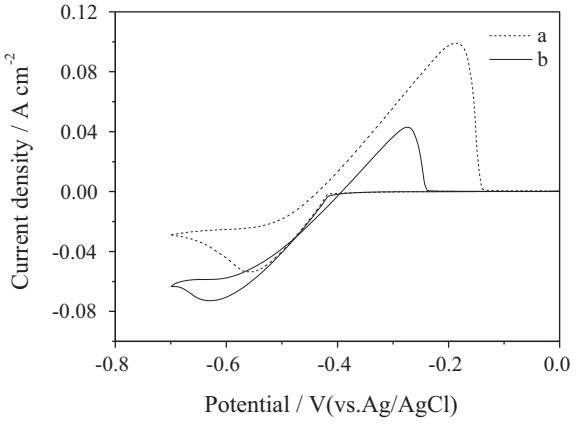

Fig. 1. Cyclic voltammograms of Pt electrode at 100 mV s^{-1} in the solution containing (a) 50 mM $SnCl_2$ + 0.1 M HCl, (b) 50 mM $SnCl_2$ + 0.1 M HNO_3.

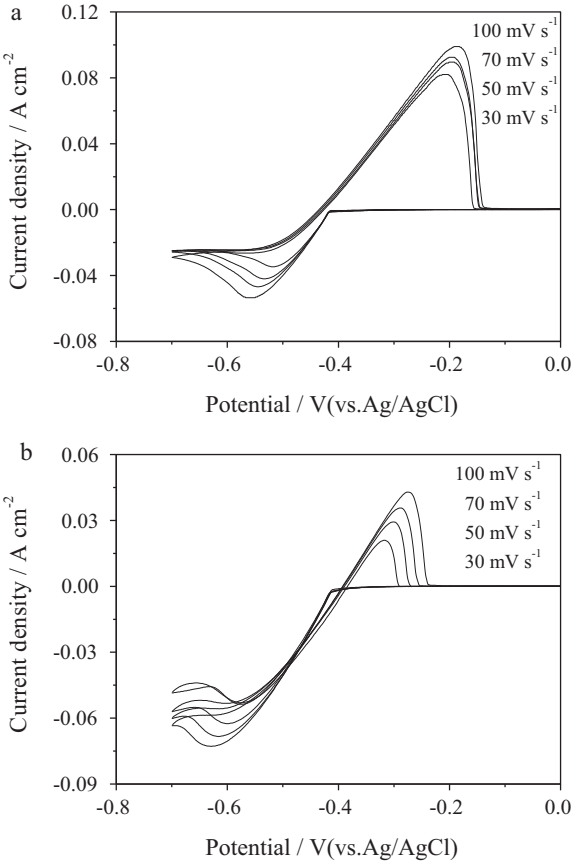

Fig. 2. Cyclic voltammograms of Pt electrode at various scan rates in the solution. (a) 50 mM $SnCl_2$ + 0.1 M HCl, (b) 50 mM $SnCl_2$ + 0.1 M HNO_3.

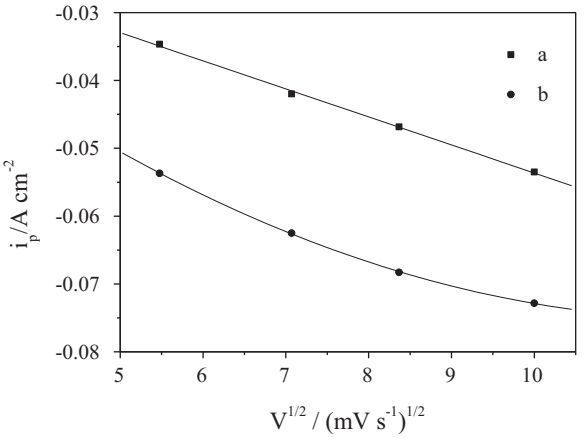

Fig. 3. Dependence of peak currents of the electroreduction reaction on the polarization rate in the solution. (a) 50 mM $SnCl_2$ + 0.1 M HCl, (b) 50 mM $SnCl_2$ + 0.1 M HNO_3.

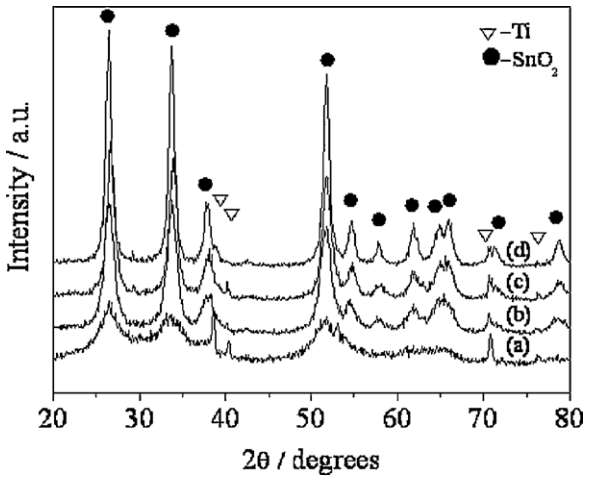

Fig. 5. XRD patterns of the nanocrystalline SnO_2 films prepared by pulse-potential technique sintered under different temperature: (a) without sintering, (b) sintered at 450 °C, (c) 550 °C and (d) 650 °C.

50 mM $SnCl_2$ + 0.1 M HNO_3. In this case, the controlling process might relate with the deposition of SnO_2.

In order to confirm the formation mechanisms of SnO_2, potentiostatic electrolysis experiments were carried out in the solution containing (a) 50 mM $SnCl_2$ + 0.1 M HCl and (b) 50 mM $SnCl_2$ + 0.1 M HNO_3. The controlled potential electrolysis was carried out on Ti metal sheet at −0.6 V (*vs.* Ag/AgCl) which was selected according to the results of cyclic voltammetry. The electrolysis was kept for 30 min. The XRD pattern of the electrodeposited film obtained in the HCl solution is shown in Fig. 4(a). The electrodeposited film was identified as metallic Sn (JCPDS database card No. 4-673). The results of XRD further confirmed that the cathodic peak in the cyclic voltammograms corresponds to the deposition of Sn metal in the HCl solution. The XRD pattern of electrodeposited film obtained in the HNO_3 solution is shown in Fig. 4 (b). The electrodeposited film was identified as the mixture of metallic Sn (JCPDS database card No. 4-673) and SnO_2 (JCPDS database card No. 21-1250). These results further showed that the simultaneous deposition of SnO_2 and metallic Sn in the HNO_3 solution which was in good agreement with the result of cyclic voltammetry.

3.2. XRD and SEM characterization of SnO_2

In order to avoid the deposition of metallic Sn, pulse-potential technique was conducted at 75 °C in the solution containing 50 mM $SnCl_2$ + 0.1 M HNO_3. The high and low potential were −0.1 V and −0.6 V, respectively, which were chosen according to the cyclic voltammetry. The pulse times were both 10 s. The first step at low potential (−0.6 V *vs.* Ag/AgCl) is the codeposition process of SnO_2 and Sn. The pulse process at the high potential of −0.1 V is expected to transform the deposited Sn to SnO_2 with the effect of anodic oxidization. The electrodeposited film was identified as SnO_2 by XRD patterns in which no significant diffraction peak was found for metallic Sn (shown in Fig. 5). Fine crystallinity is a guarantee to electron transport in the nanoporous film. So a high temperature sintering is essential. Fig. 5 also shows the XRD patterns of the nanocrystalline SnO_2 films after sintering at different temperatures. The peak width at half height of XRD patterns became shorter with the increase of sintering temperature which indicated the enhancement of crystallinity degree for SnO_2 films.

Fig. 6 shows the surface morphology image of SnO_2 film in top views. It can be seen that the SnO_2 film possesses an arborous structure (shown in Fig. 6(a)). After sintering at high temperature, most of the SnO_2 nanorods were transformed to be nanoparticles (shown in Fig. 6(b) and (c)) which could ensure a large surface area. At the same time, a few of arborous structure SnO_2 was remained. The remained arborous structure should provide a direct and rapid pathway for charge transport. The thickness of the SnO_2 film is about 15 μm.

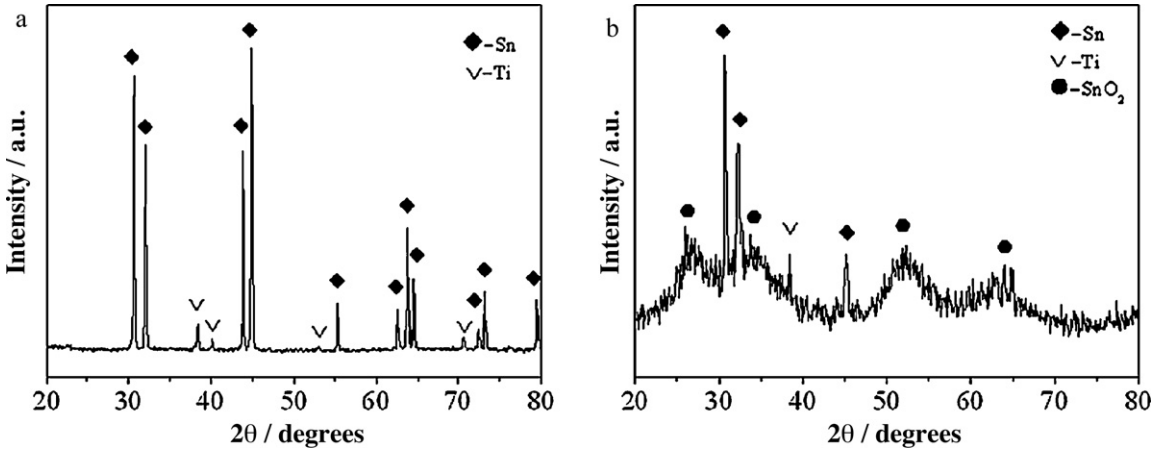

Fig. 4. XRD patterns of electrodeposited films through potentiostatic electrolysis in the solution. (a) 50 mM $SnCl_2$ + 0.1 M HCl, (b) 50 mM $SnCl_2$ + 0.1 M HNO_3.

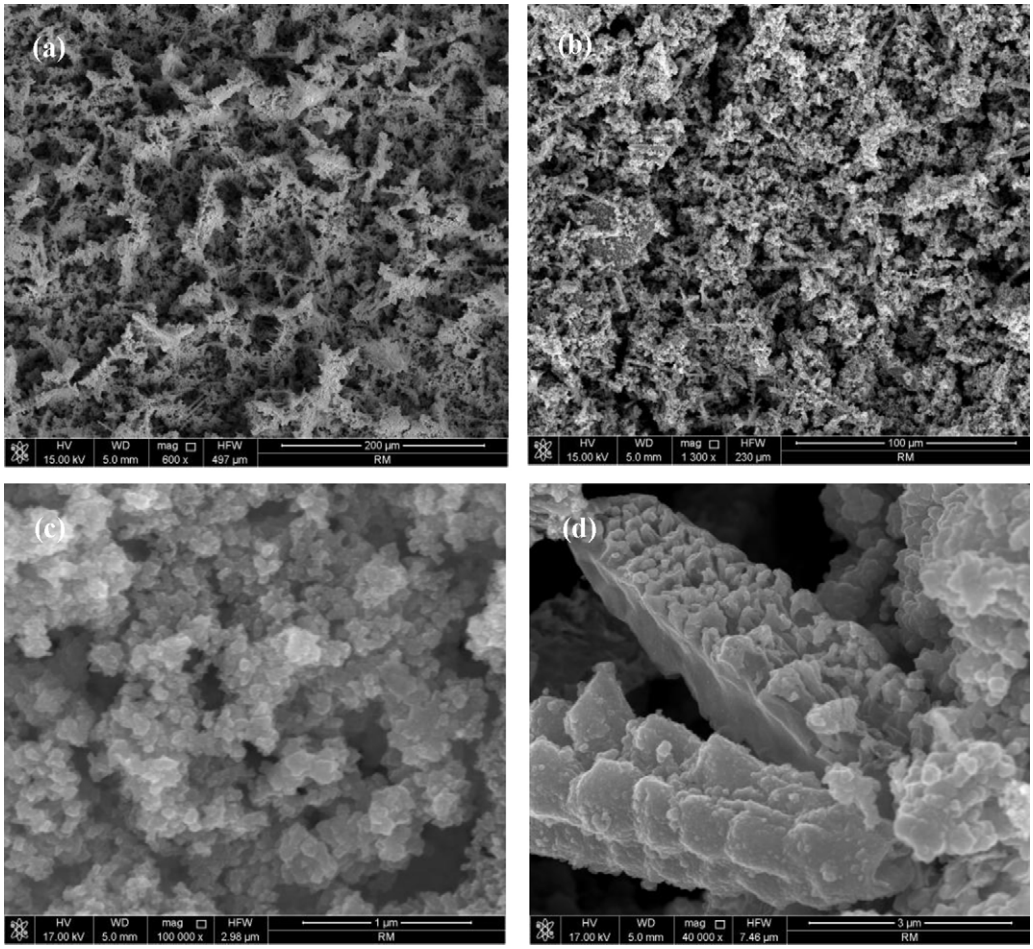

Fig. 6. SEM images of the nanocrystalline SnO_2 films prepared by pulse technique: (a) without sintering, (b), (c) and (d) sintered at 550 °C.

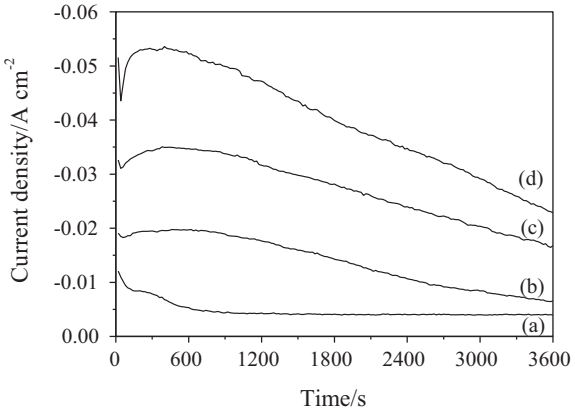

Fig. 7. The dependence of current density on the deposition time in the solution containing $SnCl_2 + HNO_3$ at −0.5 V to 0.1 V (a), −0.6 V to 0.1 V (b), −0.7 V to 0.1 V (c) and −0.8 V to 0.1 V (d) *vs.* Ag/AgCl.

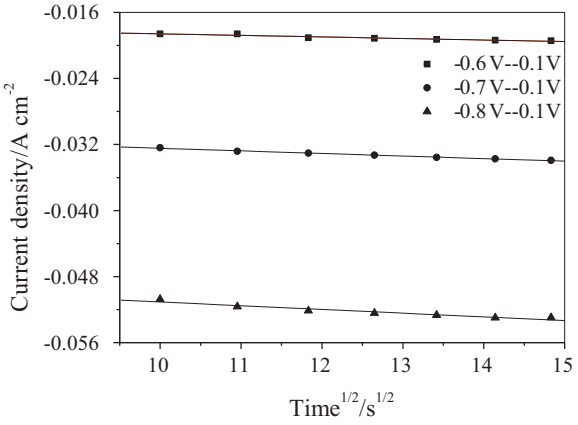

Fig. 8. Relation between I and $t^{1/2}$ constructed from the rising portion of the curves shown in Fig. 7.

3.3. Chronoamperometry analysis

In order to further investigate the nucleation and growth phenomena of SnO_2 nucleation, the dependence of current density on the deposition time was investigated (shown in Fig. 7). The deposition potential was changed from −0.5 to −0.8 V (*vs.* Ag/AgCl). When the applied potential was more negative than −0.5 V, typical curves which indicated the nucleation and growth of the SnO_2 deposit were obtained. The crystallization process is accelerated at negative potential. The first section of curves is characterized by a decrease of current with time. At this period, the double layer of cathode was charged, and at the same time the first nuclei of SnO_2 was formed. At the following section of the curve, the current increased with time because of the increasing of the effective electrode area which was caused by the nucleation and growth of SnO_2 deposit. The curve of I *vs.* $t^{1/2}$ for the rising portion of the curve at different applied potential is shown in Fig. 8. The proportionality between I and $t^{1/2}$ demonstrated that the deposition of SnO_2 involving an instantaneous nucleation process and the results of

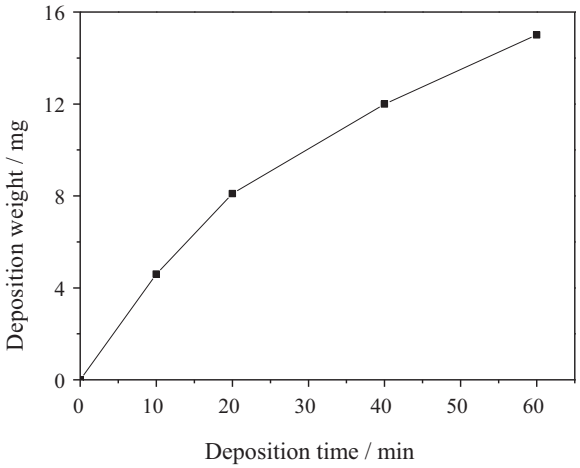

Fig. 9. Dependence of SnO_2 film mass on the deposition time.

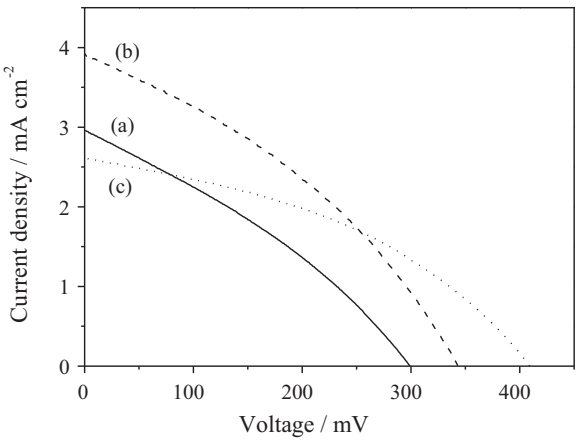

Fig. 11. The photocurrent–voltage and dark current–voltage characteristics for DSCs based on the nanocrystalline SnO_2 film sintered at different sintering temperatures: (a) 450 °C, (b) 550 °C and (c) 650 °C.

the experiments were in agree with the theory proposed by Hills [30].

Fig. 9 shows the dependence of SnO_2 mass on the deposition time. The weight of SnO_2 film increased with the deposition time. But the mass increase rate of SnO_2 slowed down. The lower deposition rate might be caused by the comparatively poor electron conductivity of SnO_2 (compared to the Ti sheets). With the increasing of the deposition time, the electrons must pass more and more SnO_2 before they can react with the oxidant in the solution which reduced the generation rate of OH^- and Sn.

3.4. Photovoltaic performance of the electrodeposited SnO_2

The SnO_2 films sintered at different temperature were sensitized with N3 dye and used to assemble DSCs. All the obtained films were deposited by the pulse technique and the deposition potential was kept at −0.6 V. In our experiments, we also investigated the deposition of SnO_2 films under various deposition potentials. When the applied potential was more negative than −0.6 V, the SnO_2 films cracked after sintering.

The UV–vis absorption spectra of bare SnO_2 film and N3-sensitized SnO_2 film are illustrated in Fig. 10(a). It can be seen that the electrodeposited SnO_2 film could adsorb a certain amount of N3 dye. However, the maximum absorption at 500 nm of pure N3 dye is shifted to 530 nm. The red shift might be attributed to the interaction between the dye molecules and semiconductor surface. The dye loading amount was determined by dissolving a known area of the film into 5 mL of NaOH solution (0.1 mol L^{-1}) and measuring its absorption spectrum. The relationship between the dye loading amount and the absorbance can be expressed by the following equation:

$$C = \frac{A}{\varepsilon \cdot S_0} V \quad (4)$$

where C is the dye loading amount, A is the absorbency at 530 nm, ε is the molar extinction coefficient, S_0 is the geometric area of the SnO_2 film, V is the volume of NaOH solution. The diffuse reflectance spectrum of the electrodeposited SnO_2 powder measured without dye and electrolyte is illustrated in Fig. 10(b). The electrodeposited SnO_2 showed relative high diffuse reflectance property.

Table 1
Performance characteristics of DSCs based on the nanocrystalline SnO_2 film under different sintering temperatures.

Temperature	J_{sc} (mA cm^{-2})	V_{oc} (mV)	FF	η (%)	Anchored dye ($\times 10^{-8}$ mol cm^{-2})
450 °C	2.96	299	0.32	0.28	1.76
550 °C	3.93	343	0.35	0.47	1.87
650 °C	2.61	409	0.40	0.43	0.59

Fig. 11 shows the current-voltage characteristics of the cells under simulated solar illumination (at 100 mW cm^{-2}) and Table 1 gives the characteristic parameters, i.e. open circuit voltage (V_{oc}), short circuit current (J_{sc}), fill factor (FF), quantity of anchored dye and overall light to electricity conversion efficiency (η). The J_{sc} increases when the sintering temperature of SnO_2 is enhanced from 450 °C and 550 °C, but it come down for higher sintering

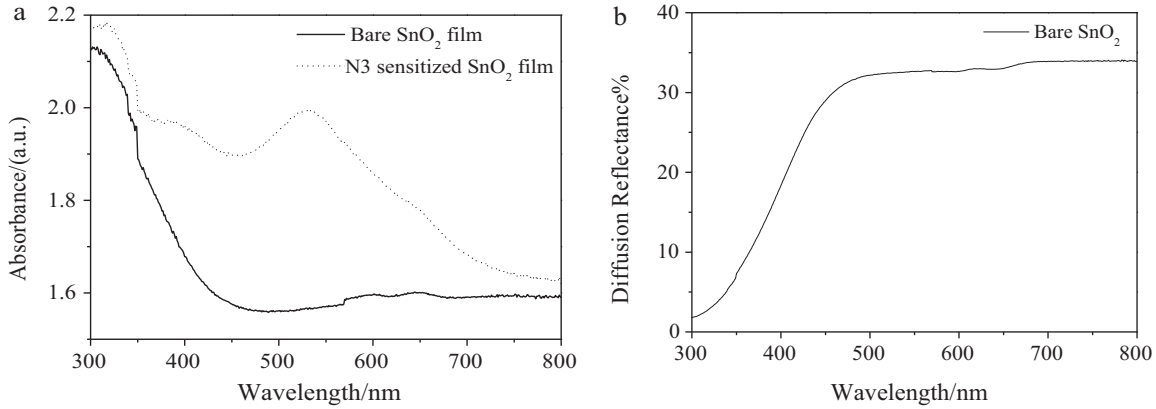

Fig. 10. UV–vis absorption spectra (a) and diffuse reflectance spectra (b) of the electrodeposited SnO_2.

temperature. The dye loading and the roughness factor of the SnO_2 films sintered at 450 °C and 550 °C showed almost no changes. The increase of J_{sc} with the sintering temperature might be contributed to the enhancement of the crystallinity (shown in Fig. 5) which facilitated the collection of the photoproduced electron. When the sintering temperature is higher than 550 °C, the dye absorption declined seriously. As a result, the J_{sc} also decreased. On the other hand, the open circuit voltage (V_{oc}) and the fill factor (FF) keep increasing with the sintering temperature of SnO_2 film which indicates that higher crystallinity has a significant influence on the charge-transport properties of the SnO_2 particles. At the sintering temperature of 550 °C, the efficiency shows a peak value of 0.47% which is comparable to that of the SnO_2 DSCs fabricated using sol–gel template synthesis [8].

4. Conclusion

SnO_2 porous films were electrodeposited at 75 °C by pulse-potential technique. The deposited film comprised with both the granular and virgate SnO_2. The deposition process was investigated with cyclic voltammetry and potentiostatic electrolysis. SnO_2 and metallic Sn were codeposited under the low pulse potential (−0.6 V *vs*. Ag/AgCl). The deposited Sn was anodic oxidized under the subsequent high pulse potential (−0.1 V *vs*. Ag/AgCl). The formation of SnO_2 possessed an instantaneous nucleation process. DSCs were fabricated using the as-deposited SnO_2 porous films. The photoelectric conversion efficiency was 0.47% with open circuit voltage 343 mV, shirt circuit current 3.93 mA cm^{-2} and fill factor 0.35.

Acknowledgements

This work was supported by the Basic and Frontier Technology Research Programs of the Department of Science & Technology of Henan Province (No. 112300410004), the Key Technologies R&D Program of Henan Province (No. 092102210005), the Nation Natural Science Foundation of China (No. 50802023) and the Research Fund of Henan University (No. 2010ZRZD07).

References

[1] B. O'Regan, M. Grätzel, Nature 353 (1991) 737–740.
[2] A. Hagfeldt, G. Boschloo, L.C. Sun, L. Kloo, H. Pettersson, Chem. Rev. 110 (2010) 6595–6663.
[3] Y. Chiba, A. Islam, R. Komiya, N. Koide, L.Y. Han, Appl. Phys. Lett. 88 (2006) 223505.
[4] M. Grätzel, Inorg. Chem. 44 (2005) 6841–6851.
[5] A. Kay, M. Grätzel, Sol. Energy Mater. Sol. Cells 44 (1996) 99–117.
[6] D.J. Fitzmaurice, M. Eschle, H. Frei, J. Phys. Chem. 97 (1993) 3806–3812.
[7] S. Rani, P. Suri, P.K. Shishodia, R.M. Mehra, Solar Energy Mater. Solar Cells 92 (2008) 1639–1645.
[8] A. Kay, M. Grätzel, Chem. Mater. 14 (2002) 2930–2935.
[9] K. Sayama, H. Sugihara, H.H. Arakawa, Chem. Mater. 10 (1998) 3825–3832.
[10] H.D. Zheng, Y. Tachibana, K. Kalantar-zadeh, Langmuir 26 (2010) 19148–19152.
[11] S. Mori, A. Asano, J. Phys. Chem. C 114 (2010) 13113–13117.
[12] H. Kim, R.C.Y. Auyeung, A. Pique, Thin Solid Films 516 (2008) 5052–5056.
[13] B.Y. Wei, M.C. Hsu, P.G. Su, P.G. Su, H.M. Lin, R.J. Wu, H.J. Lai, Sens. Actuators B: Chem. 101 (2004) 81–89.
[14] H.J. Wang, J.M. Wang, W.B. Fang, H.W.L. Liu, H.Q. Lian, Electrochem. Commun. 11 (2010) 194–197.
[15] L.M. Li, X.M. Yin, S. Liu, Y.G. Wang, L.B. Chen, T.H. Wang, Electrochem. Commun. 12 (2010) 1383–1386.
[16] M.K.I. Senevirathna, P.K.D.D.P. Pitigala, E.V.A. Premalal, et al., Sol. Energy Mater. Sol. Cells 91 (2007) 544–547.
[17] L. Liao, H.B. Lu, J.C. Li, H. He, D.F. Wang, D.J. Fu, C. Liu, W.F. Zhang, J. Phys. Chem. C 111 (2007) 1900–1903.
[18] C.L. Hsu, S.J. Chang, Y.R. Lin, P.C. Li, T.S. Lin, S.Y. Tsai, T.H. Lu, I.C. Chen, Chem. Phys. Lett. 416 (2005) 75–78.
[19] Y.Y. Xi, Y.F. Hsu, A.B. Djurišic, W.K. Chan, J. Electrochem. Soc. 155 (2008) D595–D598.
[20] K. Wessels, M. Wark, T. Oekermann, Electrochim. Acta 55 (2010) 6352–6357.
[21] B. Ferrari, R. Moreno, J. Electrochem. Soc. 147 (2000) 2987–2992.
[22] R. Sharma, R.S. Mane, S.K. Min, S.H. Han, J. Alloys Compd. 479 (2009) 840–843.
[23] C.F. Lin, H. Lin, J.B. Li, X. Li, J. Alloys Compd. 462 (2008) 175–180.
[24] H.J. An, S.R. Jang, R. Vittal, J. Lee, K.J. Kin, Electrochim. Acta 50 (2005) 2713–2718.
[25] S. Karuppuchamy, K. Nonomura, T. Yoshida, T. Sugiura, H. Minoura, Solid State Ionics 151 (2002) 19–27.
[26] S.T. Chang, I.C. Leu, M.H. Hon, J. Cryst. Growth 273 (2004) 195–202.
[27] S.T. Chang, I.C. Leu, M.H. Hon, Electrochem. Solid State Lett. 5 (2002) C71–C74.
[28] S.T. Chang, I.C. Leu, M.H. Hon, J. Alloys Compd. 403 (2005) 335–340.
[29] A.J. Bard, L.R. Faulkner, Electrochemical Methods: Fundamentals and Applications, second ed., John Wiley, New York, 2001.
[30] G.J. Hills, D.J. Schiffrin, J. Thompson, Electrochim. Acta 19 (1974) 657–670.